44th European Rotorcraft Forum
Delft, The Netherlands, 18-21
September, 2018
Paper 96

NUMERICAL SIMULATION OF DIFFERENT ROTOR DESIGNS IN HOVER AND FORWARD FLIGHT

Thomas A. Fitzgibbon, George N. Barakos, Mark A. Woodgate and Antonio Jimenez-Garcia
CFD Laboratory, School of Engineering, University of Glasgow, G12 8QQ, U.K.

Abstract

This paper presents numerical simulations of different rotor designs using the HMB3 solver of Glasgow University. The PSP blade with a swept-tapered tip, the Langley Baseline blade with a rectangular planform and the Langley BERP blade with an advanced tip shape were studied. Firstly, the three blades were examined in hover. The integrated loads were compared with experiments and show very good agreement for each of the blade designs. The effect of anhedral in hover was investigated and was found to be more beneficial for the BERP-like design, than the other blades. The PSP blade was also simulated in forward flight at three thrust coefficients. The advancing and retreating blade surface pressures were extracted and found to follow experimental data obtained using pressure transducers. The predictions for the simulated cases demonstrate the ability of the CFD method to accurately predict the performance of rotors regardless of planform geometry, or design complexity.

1 INTRODUCTION

The need of accurate CFD predictions for the design of high performance helicopter rotors is nowadays widely recognised. Past efforts using wind tunnel tests and simple aerodynamic analysis methods led to different rotor designs to be favoured across the globe. The BERP planform [1] is an example of an advanced design, whereas simpler designs such as a swept/swept-tapered or parabolic tips are also used, as discussed by Brocklehurst and Barakos [2]. The emergence of more radical rotor designs such as the Blue-Edge blade [3] or the new BOEING rotor blade [4], further highlight the progress of rotor CFD. The existing variety of designs shows that the exact planform shape of an optimum rotor is still unknown. The development of CFD methods and rapid growth in computational power, means that an optimum rotor is likely to emerge through numerical simulation. However, the ability to predict the rotor performance for advanced planforms of modern CFD methods has to be assessed. To do this, there is a growing need for high-quality validation data.

Considerable efforts have been performed within the rotorcraft research community to compare CFD predictions and real-life rotor performance. In hover, a wide range of studies were performed within the AIAA Hover Prediction Workshop since 2014 [5]. The aim of the workshop was to predict the hover performance of a rotor blade within 0.1 counts in figure of merit. The S-76 model scale rotor experiments performed by Balch [6] were used as the main test case. Comparisons were made between the workshop partners, using various solvers with different orders of accuracy, and meshing techniques. The effect of tip shape on the performance of the rotor was also investigated. This workshop showed the need for more in-depth validation data, as only integrated blade load predictions could be compared with experiments. However, surface pressure predictions, blade loads and wake geometry were also compared between the workshop participants but showed differences depending on the modelling approach [7]. The results highlighted the issues with current hover simulations such as the wake breakdown and the need for transitional turbulence models for accurate performance predictions. The need for including aeroelastic effects, as well as, facility/installation effects were also noted [8].

A number of CFD studies for rotors in forward flight are also presented in the literature. These primarily consider the UH-60A rotor due to the extensive flight test program [9] of NASA/US Army. Modelling a rotor in forward flight requires high-fidelity analyses and coupled CFD/CSD simulations. These, however are, computationally expensive but required to accurately represent the flow. Examples of CFD/CSD computations for the UH-60A rotor include simulations with OVERFLOW/CAMRAD [10], HELIOS/RCAS [11] and FUN3D/CAMRAD II [12] and many more. A variety of CFD methodologies and numerical parameters were used within these studies including the order of the spatial and time discretisation, turbulence models, and grid sizes. Other studies for rotors in forward flight include simulations for the Apache rotor using Helios coupled with CAMRAD II [13] and the ONERA 7A rotor, using elsA coupled with HOST as well as HELIOS coupled with RCAS [14]. In general, most studies are able to predict the rotor performance and rotor blade loads (especially normal forces and pitching moments) with good accuracy. The wake resolution is highly dependant on the grid size, and order of the numerical scheme used. The vibratory loads still require improvements. For better correlation with experiments and flight test data, transitional turbulence models should be used, and facility/installation effects should also be modelled.

The PSP rotor [15] is now emerging as an important test case due to available surface pressure data and planned further tests. This rotor was first tested by Wong et al. [16] in the LaRC Rotor Test Cell of the 14- by 22-ft Subsonic Tunnel, at the NASA Langley Research Center. Although one of the main objectives was to investigate the use of Pressure Sensitive Paint for experimental rotor testing, the results are also important for CFD validation purposes. The surface pressure measurements using transducers and pressure sensitive paint are reported for a range of thrust coefficients in hover and forward flight [15]. Further tests were performed by Overmeyer and Martin [17], using the same facility, who investigated hover performance and boundary layer transition effects. Future tests of the PSP rotor (with a modified blade root geometry) are planned in the National Full-Scale Aerodynamics Complex (NFAC) 80- by 120-Foot Wind Tunnel of the NASA Ames Research Center. A higher blade tip Mach number (0.65 compared to 0.58) is planned.

More radical blade designs such as the BERP planform have not yet been the subject of many scientific papers. The BERP planform is known to have superior performance compared to other blade designs at high speed forward-flight and high blade loading, while hover performance is comparable to a planform with a parabolic blade tip. Since its development [1] and with the exception of few works [18],[19],[20] not much validation has been performed for BERP blades. Optimisations of BERP-like tip geometries were performed by Johnson and Barakos [21], but the final shape was not tested in a wind tunnel. To date, the only experimental data openly-available concerning BERP-like blades was performed at NASA by Yeager et al. [22]. Integrated loads were reported in hover and forward flight. There is no experimental data regarding the surface pressure distributions, sectional loads and wake geometry for this type of blade. The exact benefits of this type of blade have not yet been quantified in literature.

In this paper we present the simulations for the PSP rotor, Langley BERP and Langley Baseline blades designs. Firstly, the three blades were examined in hover. The integrated loads are compared with experimental data from Overmeyer et al. [17] for the PSP rotor, and Yeager et al. [22] for the Langley BERP and Baseline blades. The effect of tip anhedral is studied for the Langley BERP and Baseline blades. The PSP blade is also examined in forward flight at three thrust coefficients as a continuation of the work performed by Jimenez and Barakos [23]. Comparisons are made with available experimental data from Wong et al. [15] in terms of surface pressures on the advancing and retreating blades. Based on the results, the accuracy of the CFD method is assessed for different planform designs.

2 CFD METHOD

The Helicopter Multi-Block (HMB) [24, 25] code is used as the CFD solver for the present work. It solves the Unsteady Reynolds Averaged Navier-Stokes (URANS) equations in integral form using the Arbitrary Lagrangian Eulerian (ALE) formulation for time-dependent domains, which may include moving boundaries. The Navier-Stokes equations are discretised using a cell-centred finite volume approach on a multi-block grid. The spatial discretisation of these equations leads to a set of ordinary differential equations in time,

$$\frac{d}{dt}(\boldsymbol{W}_{i,j,k}\, V_{i,j,k}) = -\boldsymbol{R}_{i,j,k}(\boldsymbol{W}) \tag{1}$$

where i, j, k represent the cell index, $\boldsymbol{W}$ and $\boldsymbol{R}$ are the vector of conservative flow variables and flux residual respectively, and $V_{i,j,k}$ is the volume of the cell i, j, k. To evaluate the convective fluxes, the Osher[26] approximate Riemann solver is used, while the viscous terms are discretised using a second order central differencing spatial discretisation. The Monotone Upstream-centred Schemes for Conservation Laws, which is referred to in the literature as the MUSCL approach and developed by Leer [27], is used to provide high-order accuracy in space. The HMB solver uses the alternative form of the Albada limiter [28] being activated in regions where a large gradients are encountered mainly due to shock waves, avoiding the non-physical spurious oscillations. An implicit dual-time stepping method is employed to performed the temporal integration, where the solution is marching in pseudo-time iterations to achieve fast convergence, which is solved using a first-order backward difference. The linearised system of equations is solved using the Generalised Conjugate Gradient method with a Block Incomplete Lower-Upper (BILU) factorisation as a pre-conditioner [29]. To allow an easy sharing of the calculation load for parallel job, a multi-block structured meshes are used. Various turbulence models are available in HMB solver, including several one-equation, two-equation, three-equation, and four-equation turbulence models. Furthermore, Large-Eddy Simulation (LES), Detached-Eddy Simulation (DES) and Delay-Detached-Eddy Simulation (DDES) are also available. For this study, the fully-turbulent Wilcox's k-ω-SST model from Menter [30] is employed. The Overset Grid Method is used [31] for ease of grid generation and to allow for the relative motion between mesh components in forward flight cases. Information about the implementation of the overset grid method in HMB can be found in [31].

3 NUMERICAL SETUP AND TEST CONDITIONS

3.1 Blade Geometries

The four-bladed PSP rotor has an aspect ratio (R/c) of 12.2, a geometric solidity of 0.1033 and a nominal twist of -14 degrees. The blade planform has been generated using three aerofoils. First, the RC(4)-12 aerofoil was used up to 65% R, then, the RC(4)-10 aerofoil from 70% R to 80% R, finally, the RC(6)-08 aerofoil was used from 85% R to the tip. The aerodynamic characteristics of these aerofoils can be found in [32, 33]. The PSP model rotor has a swept-tapered tip as shown in Figure 1.

The Langley BERP and Baseline blades were tested at model scale by Yeager et al. [22]. The two blades have the same linear twist, radius, aerofoils and only differ by the tip shape and chord length, which was changed to match the rotor thrust-weighted solidity. Due to the different root chords, the blade aspect ratios are slightly different (13.76 for the BERP-like and 12.62 for the Baseline blade), and hence the geometric solidity of the Baseline rotor is higher than for the BERP-like blade (0.101 compared to 0.096). Both rotors use the RC(4)-10 aerofoil section inboards of the tip section whereas the RC(3)-07 section is used across the blade tip. The outboard section coordinates are not reported in the literature, however the use of the RC(3)-08 section leads to an increase in rotor blade thickness near the BERP-like tip, hence the thickness of aerofoil was scaled. The characteristics of these two aerofoils are given by Noonan [32],[33]. The aerofoil transition occurs between 0.84R and 0.866R. Both blades have a linear twist of approximately 9 degrees with a constant twist across the blade tip. An additional Langley Baseline geometry was generated with a continued twist across the blade tip. The blade planform geometries and twist distributions are shown in Figure 2. In terms of geometry, there are a few unknowns. The exact shape of the BERP-tip along with its thickness distribution is not fully defined [22]. Furthermore, the curvature of the aerofoil transition region is also not known. Finally, two geometries with 15 degrees of anhedral are generated. The anhedral is initiated from the start of the raked section of the BERP tip (0.945R).

3.2 Computational setup

The chimera technique is used for evaluations of the PSP, Langley BERP and Langley Baseline blades. For all cases, the isolated rotors were simulated without modelling the fuselage, test stand or facility walls. The rotors were modelled as rigid as the tests were performed at model scale and the blades were fairly stiff. Multi-block structured meshes were generated for each of the cases. In hover, only a quarter of the computational domain was meshed, assuming periodic conditions for the flow field in the azimuthal direction. This assumption is valid if the wake generated by the rotor is assumed periodic and the blades do not experience deep stall. A source/sink model is used for the simulations with a Froude boundary condition imposed at the inflow and outflow. A typical computational domain is shown in Figure 3. The distances between the rotor blades and the farfield boundaries, as well as inflow/outlfow surfaces in hover are based on experience from previous studies using the HMB3 solver [23]. In forward flight, the full rotor disk with four blades was simulated as the flow is unsteady. A hub was also included in the computational domain and modelled as a generic ellipsoidal surface. For the blades, a C-topology around the leading edge of the blade was selected, whereas an H-topology was employed at the trailing edge. For the Langley BERP blade, an O-grid is used around the tip of the blade. The topologies of the meshes for the three blades are shown in Figure 3. The grids for the Langley BERP and Baseline blades with anhedral are generated using a mesh deformation method (based on Inverse Distance Weighting). The grid sizes for the PSP, Langley BERP and Baseline rotor blades in hover and forward flight are shown in Table 1. All meshes have a wall distance of $1.0 \cdot 10^{-5}$ c_{ref}. Typically 220-260 points are used around the aerofoil with 160-200 points in the spanwise direction.

3.3 Test conditions

In hover, the PSP blade was simulated at a blade-tip Mach number 0.58 at a range of thrust coefficients. These conditions were used by Overmeyer et al. [17], who measured integrated blade loads for free and fixed transition conditions. The tests were performed in the Rotor Test Cell at the NASA Langley Research Center 14×22 Foot Subsonic Wind Tunnel. The rotor was installed on the modified ROtor BOdy Interaction fuselage (ROBIN Mod7) and was tested in Out of Ground Effect (OGE) conditions. The Reynolds number, based on the reference blade chord c_{ref} of 5.45 inches and on the blade-tip speed, was $1.94 \cdot 10^{6}$. The PSP blade was also simulated in forward flight at three thrust coefficients and $\mu = 0.35$. This corresponds to the conditions used by Wong et al. [15] who performed experiments for this blade in forward flight. The freestream Mach number was 0.2 with a free-stream Reynolds number of 6.98×10^5. A matrix trimming routine [24] based on the Blade Element Theory for computing the elements of the sensitivity matrix was used for the forward flight computations to achieve the target thrust and reduce rolling and pitching moments. For these computations, 0.25 deg azimuthal steps were used along with the $k\omega - SST$ turbulence model.

The Langley BERP and Baseline blades were tested at a blade tip Mach number of 0.628 in a Freon-12 medium which has a higher density than air, allowing model scale tests at Reynolds numbers closer to full scale. The Reynolds numbers were calculated based on a Freon density of 3.09227 kg/m^2 and dynamic viscosity of $12.357 \times 10^-6 Pa/s$. The reference velocity was calculated based on a speed of sound equal to 153.924 m/s (giving a value of $V_{ref} = 95.664 m/s$). The reference length used was the chord of the first aerodynamic section at 21.5% R (0.10378m for Langley BERP and 0.11314m for Langley Baseline). A specific heat ratio of 1.128 (compared to 1.4 for air) was also used for the CFD simulations. The hover experiments were performed in minor ground effect of z/d=0.83. Here, the Langley BERP and Baseline blades are simulated out of ground effect and at four collectives in hover. The effect of a 15 degree parabolic anhedral was examined at a single collective of 10.5 degrees.

Table 2 summarizes the computed cases in hover, whereas the computations in forward flight are presented in Table 3.

4 RESULTS

4.1 Hover

4.1.1 PSP blade

The predicted integrated loads for the PSP rotor are shown in Figure 4 for six blade pitch angles. The results are compared with experimental data from Overmeyer et al. [17] for fixed-transition, at 5% c, upper and lower (run 156). The momentum theory predictions are also included for an induced power factor k_i of 1.15 and overall profile drag coefficient C_{D0} of 0.01. Three sets of published CFD simulations are also included for direct comparison. Green lines correspond to Wong [34], using the unstructured solver FUN3D and the fixed Spalart-Allmaras as turbulence model [35]. Vieira *et al.* [36] employed the commercial software Star-CCM+ (red triangle symbols) with the same turbulence model. Blue diamond symbols correspond to numerical simulations performed by Rohit [37] with the structured OVERFLOW solver, fully turbulent and isolated rotor (without fuselage) (see Rohit [37], Figure 10).

At low thrust $C_T/\sigma < 0.06$, it can be seen that all CFD computations are in close agreement with experiments. Note that at low thrust, the Figure of Merit (FoM) shows low values as consequence of the higher contribution of the profile drag, which is relatively easy to predict. At medium and high thrust $0.06 < C_T/\sigma < 0.1$, results with FUN3D, OVERFLOW and Star-CCM+ overpredict the values of FoM, while HMB3 slightly underpredicts the FoM. As an example, at thrust coefficient of $C_T/\sigma = 0.0828$, FUN3D, OVERFLOW, Star-CCM+, and HMB3 shows a discrepancy of +1.7,+0.8,+2.5, and -0.4 counts of FoM respect to the experiments. Note that the OVERFLOW and FUN3D values reported here were extracted from the papers ([37], Figure 10) and ([34], Figure 18), respectively, which may introduce a source of discrepancy when compared. Regarding the maximum thrust coefficient measured in the wind tunnel $C_T/\sigma < 0.096$, HMB3 results show maximum discrepancies of -2 counts with respect to the experiments. Rohit ([37], Figure 10) evaluated the effect of rotor installation on the FoM, and it was found that the installed-rotor FoM presents a higher values (around 1.4 counts of FoM) when compared with the isolated rotor at $C_T/\sigma \approx 0.094$, which perhaps the main source of discrepancy, at high thrust, between HMB3 and experiments. The surface pressure comparisons with experimental data are reported by Jimenez and Barakos [23]. These are presented here in Figures 5-6 at two radial stations (r/R=0.93 and 0.99), where the C_P is computed based on the local velocity. The experimental data measured the C_P distributions using pressure transducers and the PSP technique. Reasonable agreement is seen by both methods. The CFD results are able to predict the overall pressure distributions with good accuracy. At higher thrust levels, the C_P is slighly overpredicted close to the leading edge, however, the trailing edge C_P is well captured.

4.1.2 Langley Baseline and BERP blades

Figure 7 presents the performance of the Langley BERP and Baseline blades in hover. The data obtained from CFD simulations is compared with experimental data from Yeager et al. [22]. The hover performance predictions show very good agreement with experimental data. Each of the CFD resulting curves fits well within the scatter of the experimental data. The trends of each curve are captured well, with the Langley BERP blade figure of merit curve flattening out at higher thrust coefficients. For the Langley Baseline blade, it was found that continuing the blade twist across the blade tip improves the performance of the rotor in terms of FoM by approximately 1-2 counts. As predicted by experiments, the FoM of the BERP blade is lower than for the Baseline blade across the whole examined thrust envelope. As the collective increases, the difference in thrust coefficient between the BERP and Baseline blades increases. At a high thrust setting, the performance of the BERP blade surpasses the Baseline blade with flat twist. This is in agreement with literature [18],[1] and proves the high angle of attack performance of the BERP blade. The BERP blade is able to operate at high loading conditions without major losses in thrust. In terms, of the hover modelling, it can be stated that the current methodology is sufficient when compared to the experimental performance predictions. Higher order methods and larger grid sizes are only justified when comparing with experimental data sets with less uncertainties. To further, validate these results, there is a need for a more comprehensive experimental data set including surface pressure, sectional loads and wake geometry data.

Next, the effect of anhedral for the two blades is assessed. The performance results at 10.5 degrees collective are presented in Table 4. Anhedral is found to improve the hover performance of a blade in terms of FoM and was more beneficial for the Langley BERP blade than the Langley Baseline blade. The blade anhedral redistributed the loading along the blade leading to offloading of the blade tip and higher loading inboard as can be seen in Figure 8. This leads to a more optimal induced lift distribution and reduced overall torque. In fact, the blade anhedral acts similarly as additional negative twist on the blade loading distribution. The differences in blade loading for the blades with and without anhedral are noticeably lower for the Langley Baseline blade. For the Langley BERP blade, a reduced suction at the blade tip caused by the formation of the tip vortex can be observed. The suction is increased, however, in the blade notch region. The reasoning behind these changes in blade loading due to anhedral mainly come from the fact that the preceding blade vortex induces velocities that are oriented in a tangential manner to the curved blade tip for the blades with anhedral.

4.2 Forward flight

4.2.1 PSP blade

The PSP main rotor was simulated in medium-speed forward flight. The rotor advance ratio was μ= 0.35, the freestream Mach number 0.2 and the blade tip Mach number equal to 0.58. Experimental data for the surface pressure predictions was obtained by Wong et al. [15] at four thrust conditions. Here, we present the forward flight predictions at $C_T = 0.004$, $C_T = 0.006$ and $C_T = 0.008$ as a continuation of the work performed in [23]. The trim states are specified in Table 5. Note that the negative Fourier series is used with the HMB solver. The integrated loads for these cases are not presented due to lack of available experimental data.

The disk loads for the three cases are presented in Figure 9. The normal force indicates a thrust loss region on the advancing side for all three cases, which reduces with increasing thrust coefficient. As the thrust coefficient goes up, the front and back of the disk produce even higher normal forces. The reversed flow region can also be seen in the inboard region of the retreating side. The torque coefficient distributions show regions of high torque at the back of the disk. With increasing thrust, higher torque is also observed on the retreating side and front of the rotor disk. On the advancing blade, regions of negative torque were observed when only the pressure term was accounted for. In this region the skin friction has a large contribution to the total torque. The moment distribution does not vary greatly with thrust coefficient. A slightly higher nose-up (positive) moment can be seen on the retreating side and back of the disk at higher thrust coefficients.

The surface pressure predictions are compared with experimental data from Wong et al. [15] at the station r/R=0.99 at the Advancing and Retreating Blade Sides (ABS and RBS) of the rotor for the three simulated thrust coefficients. Two techniques were used to measured C_P distributions, the Kulite pressure transducers (square symbols) and the non-intrusive PSP technique (dashed lines) in Figure 10. CFD results were extracted at the ABS ($\psi = 100°$) and RBS ($\psi = 260°$), while experimental C_P were measured at $101°$ and $262°$. Note that the PSP data was sampled at the 98.2%R station. Regarding the ABS side, a large discrepancy is seen by both techniques. CFD results are able to predict the overall distribution of C_P and follow quite well the Kulite C_P data. The same behaviour is found at the retreating side where CFD predictions are in close agreement with the Kulite data too.

Finally, the PSP rotor flowfield is visualized using the Q-criterion [38] (value of 0.002) at two thrust coefficients of $C_T = 0.004$ and $C_T = 0.008$ and is presented in Figure 11. The main wake structures are well resolved for each of the cases. For both cases, the wake is fastly convected downstream due to the high advance ratio. For the high thrust case, a higher downwash is produced by the rotor, hence the wake is convected further downwards in the axial direction compared to the low thrust case. The wake structures away from the rotor are better resolved for the high thrust case, as a higher number of mesh points is used in the vicinity of the rotor. As both cases were performed at the same advance ratio, the flow structures are fairly similar.

5 CONCLUSIONS AND FUTURE WORK

The results presented have shown that the CFD method is able to predict the hover performance of a rotor blade, regardless of planform geometry, with good accuracy. The current methodology has shown to give good predictions at low computational expense. To gain greater confidence in the CFD predictions, there is a growing need for a more comprehensive experimental data set including surface pressures, sectional loads and wake geometry. The effect of anhedral is well captured within the CFD simulations and has proven to be beneficial in hover, especially for BERP-like planforms. For the PSP blade in forward flight, the surface pressure predictions on the advancing and retreating blades showed good agreement with experimental data from the Kulite transducers, but not the PSP technique. Future work includes, assessment of the impact of transition on the hover performance of the PSP rotor.

6 Acknowledgments

This work is funded by DSTL (Defence Science and Technology Laboratory) and is part of the TTCP AER CP13A.1 Program. Results were obtained using the EPSRC funded ARCHIE-WeSt High Performance Computer (www.archie-west.ac.uk). EPSRC grant no. EP/K000586/1. This work used the Cirrus UK National Tier-2 HPC Service at EPCC (http://www.cirrus.ac.uk)

7 REFERENCES

References

[1] Perry, F., "Aerodynamics of the World Speed Record," *43rd Annual Forum of the American Helicopter Society*, 1987.

[2] Brocklehurst, A. and Barakos, G., "A review of helicopter rotor blade tip shapes," *Progress in Aerospace Sciences*, Vol. 56, 2013, pp. 35 – 74.

[3] Rauch, P., Gervais, M., Cranga, P., Baud, A., Hirsch, J., Walter, A., and Beaumier, P., "Blue Edge (TM): The Design, Development and Testing of a New Blade Concept," *American Helicopter Society 67th Annual Forum*, 2011.

[4] Boeing, "New Chinook Composite Blades Proven," `http://www.boeing.com/features/2017/01/chinook-blades-01-17.page`, 2017, [Online; accessed 22-March-2018].

[5] Hariharan, N., Egolf, T., and Sankar, L., "Simulation of Rotor in Hover: Current State and Challenges," *AIAA SciTech Forum, 52th Aerospace Sciences Meeting*, 2014.

[6] Balch, D. and J.Lombardi, "Experimental Study of Main Rotor Tip Geometry and Tail Rotor Interactions in Hover, Vol I - Text and Figures," Tech. rep., National Aeronautics and Space Administration, 1985, NASA-CR-177336-Vol-1.

[7] Hariharan, N., Narducci, R., Reed, E., and Egolf, T., "Helicopter Aerodynamic Modeling of Rotor with Tip-Shape Variations: AIAA Standardized Hover Evaluations," *AIAA SciTech Forum, 54th Aerospace Sciences Meeting*, 2016.

[8] Egolf, T., Hariharan, N., Narducci, R., and Reed, E., "AIAA Standardized Hover Simulation: Hover Performance Prediction Status and Outstanding Issues," *AIAA SciTech Forum, 55th Aerospace Sciences Meeting*, 2017.

[9] Bousman, W. and Kufeld, R., "UH-60A Airloads Catalog," Tech. rep., National Aeronautics and Space Administration, 2005, NASA/TM-2005-212827.

[10] Ahmad, J. and Chaderjian, N., "High-Order Accurate CFD/CSD Simulation of the UH-60 Rotor in Forward Flight," *29th AIAA Applied Aerodynamics Conference*, 2011.

[11] Sitaraman, J., Potsdam, M., Jayaraman, B., Datta, A., Wissink, A., Mavriplis, D., and Saberi, H., "Rotor Loads Prediction Using Helios: A Multi-Solver Framework for Rotorcraft CFD/CSD Analysis," *49th AIAA Aerospace Sciences Meeting including the New Horizons Forum and Aerospace Exposition*, 2011.

[12] Biedron, R. and Lee-Rausch, E., "Blade Displacement Predictions for the Full-Scale UH-60A Airloads Rotor," *American Helicopter Society 70th Annual Forum*, 2014.

[13] Narducci, R. and Tadghighi, H., "An Assessment of $CREATE^{TM} - AV$ Helios for Apache Hover and Forward Flight Simulations ," *AIAA SciTech Forum, 54th AIAA Aerospace Sciences Meeting*, 2016.

[14] Yeo, H., Postsdam, M., Ortun, B., and Van Truong, K., "High-Fidelity Structural Loads Analysis of the ONERA 7A Rotor," *Journal of Aircraft*, Vol. 54, No. 5, 2017, pp. 1825–1839.

[15] Wong, O., Watkins, A., Goodman, K., Crafton, J., Forlines, A., Goss, L., Gregory, J., and Juliano, T., "Blade Tip Pressure Measurements using Pressure Sensitive Paint," *American Helicopter Society 68th Annual Forum*, 2012.

[16] Wong, O., Watkins, A., and Ingram, J., "Pressure Sensitive Paint Measurements on 15% Scale Rotor Blades in Hover," *35th AIAA Fluid Dynamics Conference and Exhibit*, 2005.

[17] Overmeyer, A. and Martin, P., "Measured Boundary Layer Transition and Rotor Hover Performance at Model Scale," *AIAA SciTech Forum, 55th AIAA Aerospace Sciences Meeting*, 2017.

[18] Scott, M., Sigl, D., and Strawn, R., "Computational and Experimental Evaluation of Helicopter Rotor Tips for High-Speed Flight," *Journal of Aircraft*, Vol. 28, No. 6, 1991, pp. 403–409.

[19] Srinivasan, G., Raghavan, V., and Duque, E., "Flowfield Analysis of Modern Helicopter Rotors in Hover by Navier-Stokes Method," *International Technical Specialists Meeting on Rotorcraft Acoustics and Rotor Fluid Dynamics*, 1991.

[20] Duque, E., "A Numerical Analysis of the British Experimental Rotor Program Blade," *45th Annual Forum of the American Helicopter Society*, 1989.

[21] Johnson, C. and Barakos, G., "Optimizing Rotor Blades with Approximate British Experimental Rotor Programme Tips," *Journal of Aircraft*, Vol. 51, No. 2, 2014.

[22] Yeager Jr, W., Noonan, K., Singleton, J., Wilbur, M., and Mirick, P., "Performance and Vibratory Loads Data From a Wind-Tunnel Test of a Model Helicopter Main-Rotor Blade With a Paddle-Type Tip," Tech. rep., National Aeronuatics and Space Administration, 1997, NASA-TM-4754.

[23] Jimenez-Garcia, A. and Barakos, G., "Numerical Simulations on the PSP Rotor Using HMB3," *AIAA SciTech Forum, 56th Aerospace Sciences Meeting*, 2018.

[24] Steijl, R., Barakos, G. N., and Badcock, K., "A framework for CFD analysis of helicopter rotors in hover and forward flight," *International Journal for Numerical Methods in Fluids*, Vol. 51, No. 8, 2006, pp. 819–847, DOI: 10.1002/d.1086.

[25] Steijl, R. and Barakos, G. N., "Sliding mesh algorithm for CFD analysis of helicopter rotor-fuselage aerodynamics," *International Journal for Numerical Methods in Fluids*, Vol. 58, No. 5, 2008, pp. 527–549, DOI: 10.1002/d.1757.

[26] Osher, S. and Chakravarthy, S., "Upwind schemes and boundary conditions with applications to Euler equations in general geometries," *Journal of Computational Physics*, Vol. 50, No. 3, 1983, pp. 447–481, DOI: 10.1016/0021-9991(83)90106-7.

[27] van Leer, B., "Towards the ultimate conservative difference scheme. V.A second-order sequel to Godunov's Method," *Journal of Computational Physics*, Vol. 32, No. 1, 1979, pp. 101–136, DOI: 10.1016/0021-9991(79)90145-1.

[28] van Albada, G. D., van Leer, B., and Roberts, W. W., "A Comparative Study of Computational Methods in Cosmic Gas Dynamics," *Astronomy and Astrophysics*, Vol. 108, No. 1, 1982, pp. 76–84.

[29] Axelsson, O., *Iterative Solution Methods*, Cambridge University Press: Cambridge, MA, 1994.

[30] Menter, F. R., "Two-Equation Eddy-Viscosity Turbulence Models for Engineering Applications," *AIAA Journal*, Vol. 32, No. 8, 1994, pp. 1598–1605, DOI: 10.2514/3.12149.

[31] Jarkowski, M., Woodgate, M., Barakos, G. N., and Rokicki, J., "Towards consistent hybrid overset mesh methods for rotorcraft CFD," *International Journal for Numerical Methods in Fluids*, Vol. 74, No. 8, 2014, pp. 543–576, DOI: 10.1002/fld.3861.

[32] Noonan, K. W., "Aerodynamic Characteristics of Two Rotorcraft Airfoils Designed for Application to the Inboard Region of a Main Rotor Blade," NASA TP-3009, U.S. Army Aviation Systems Command, TR-90-B-005, July 1990.

[33] Noonan, K. W., "Aerodynamic Characteristics of a Rotorcraft Airfoil Designed for the Tip Region fo a Main Rotor Blade," NASA TM-4264, U.S. Army Aviation Systems Command, TR-91-B-003, May 1991.

[34] Wong, T.-C., "Application of CREATE^{TM}-AV Helios in an Engineering Environment: Hover Prediction Assessment," *Proceedings of the 55th Aerospace Sciences Meeting*, AIAA-2017-1667, Grapevine, Texas, 2017, pp. 1–26.

[35] Spalart, P. R. and Allmaras, S., "A One-Equation Turbulence Model for Aerodynamic Flows," *La Recherche Aérospatiale*, , No. 1, 1994, pp. 5–21.

[36] Vieira, B. A. O., Kinzel, M. P., and Maughmer, M. D., "CFD Hover Predictions Including Boundary-Layer Transition," *Proceedings of the 55th Aerospace Sciences Meeting*, AIAA-2017-1665, Grapevine, Texas, 2017, pp. 1–16.

[37] Rohit, J., "CFD Performance and Turbulence Transition Predictions on an Installed Model-scale Rotor in Hover," *Proceedings of the 55th Aerospace Sciences Meeting*, AIAA-2017-1871, Grapevine, Texas, 2017, pp. 1–29.

[38] Jeong, J. and Hussain, F., "On the Identification of a Vortex," *Journal of Fluid Mechanics*, Vol. 285, No. 1, 1995, pp. 69–94, DOI: 10.1017/S0022112095000462.

8 TABLES AND FIGURES

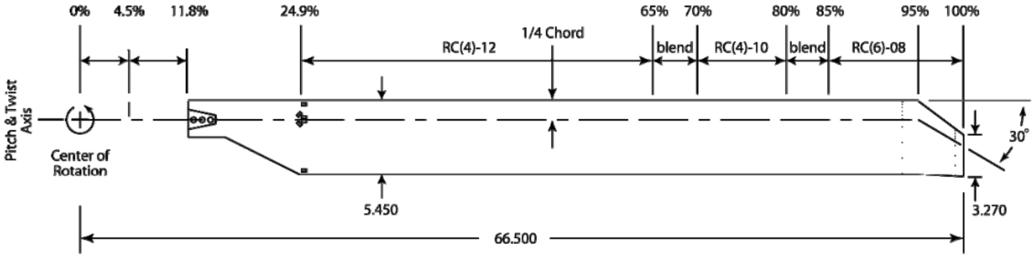

Figure 1: Planform of the PSP model rotor with a 60% taper and 30° swept tip [15].

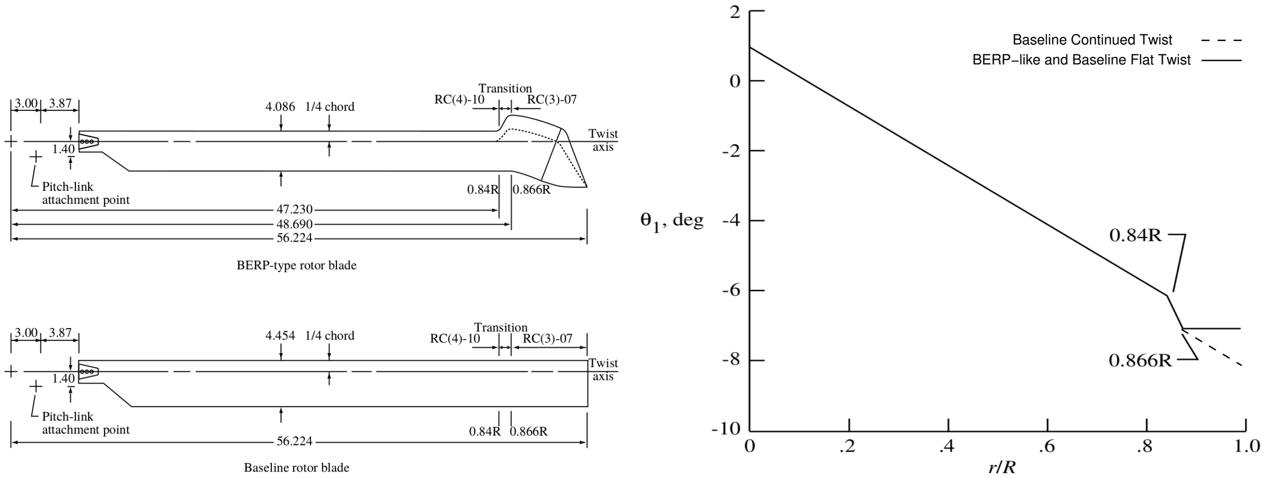

Figure 2: Blade planforms and twist distributions of the Langley BERP and Baseline blades [22].

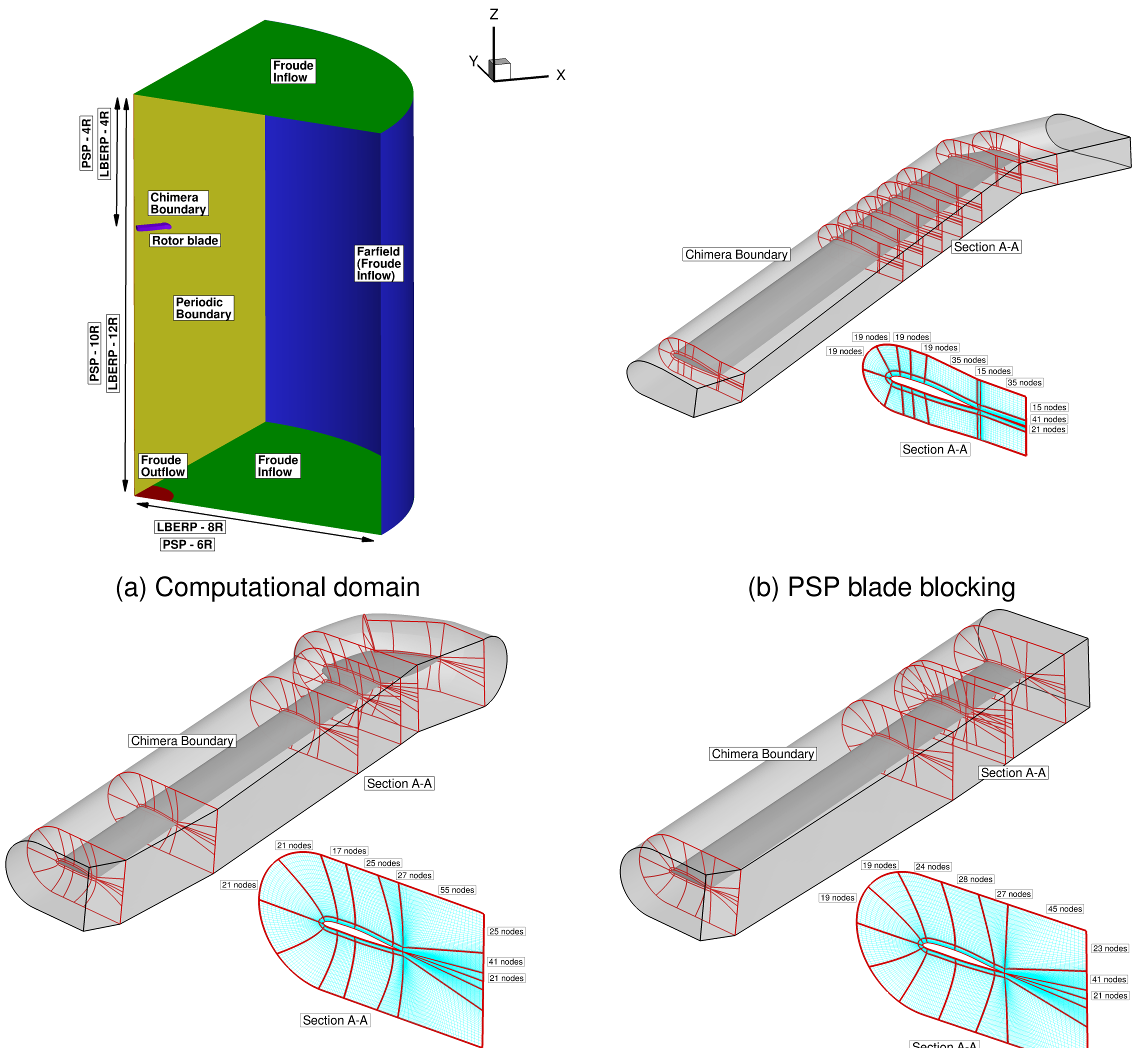

(a) Computational domain

(b) PSP blade blocking

(c) Langley BERP blade blocking

(d) Langley Baseline blade blocking

Figure 3: Computational domain in hover and blade mesh topologies for the Langley Baseline, Langley BERP and PSP blades.

Table 1: Grid sizes in millions of cells for the simulated PSP, Langley Baseline and Langley BERP blades in hover and forward flight.

Blade & Condition	**Foreground Mesh**	**Background Mesh**	**Total mesh size**
Langley Baseline (hover)	3.9M	4.9M	8.8M
Langley BERP (hover)	4.6M	4.9M	9.5M
PSP (hover)	4.8M	7.2M	12M
PSP (forward flight)	11.5M	20M	31.5M

Table 2: Computational cases in hover for the Langley BERP and Baseline blades, const.=constant, cont.=continued, anh=anhedral,Re No.=Reynolds Number, TM=Turbulence model, SST=Shear Stress Transport.

Blade	θ_{75}	β_0	M_{TIP}	Re No.	TM
LBERP	9^o, 10.5^o, 12^o, 13.5^o	0^o	0.628	2.51×10^6	$k\omega - SST$
LBASELINE (const. twist)	9^o, 10.5^o, 12^o,13.5^o	0^o	0.628	2.74×10^6	$k\omega - SST$
LBASELINE (cont. twist)	9^o, 10.5^o, 12^o	0^o	0.628	2.74×10^6	$k\omega - SST$
LBERP, 15^o anh	10.5^o	0^o	0.628	2.51×10^6	$k\omega - SST$
LBASELINE (const. twist), 15^o anh	10.5^o	0^o	0.628	2.74×10^6	$k\omega - SST$
PSP	4^o, 6.58^o, 8.48^o, 9.46^o, 10.3^o, 12^o	0^o, 1.39^o, 2.44^o, 3.02^o, 3.5^o, 0^o	0.58	1.92×10^6	$k\omega - SST$

Table 3: Computational cases in forward flight for the PSP blade in forward flight.

C_T^{USA}	μ	M_∞	Re No.	TM
0.004	0.35	0.2030	6.98×10^5	$k\omega - SST$
0.006	0.35	0.2030	6.98×10^5	$k\omega - SST$
0.008	0.35	0.2030	6.98×10^5	$k\omega - SST$

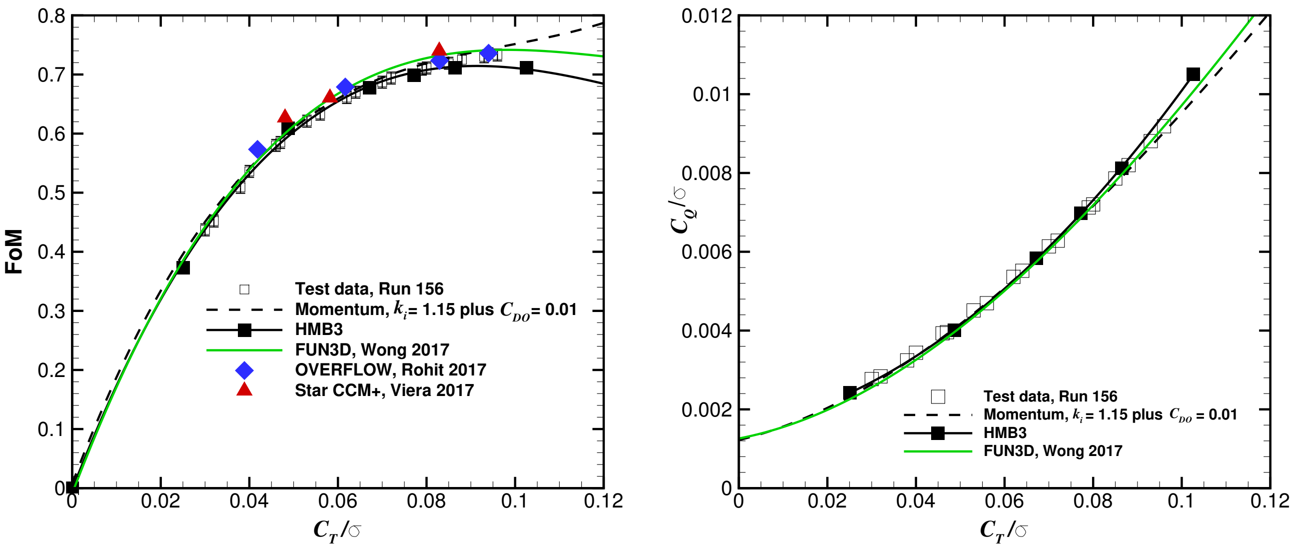

(a) C_T/σ-FoM.

(b) C_T/σ-C_Q/σ

Figure 4: Integrated blade loads for the PSP model rotor at blade-tip Mach number of 0.585. Comparisons with published CFD data: FUN3D [34] (green lines), OVERFLOW [37] (blue diamond symbols), Star CCM+ [36] (red triangle symbols) and experimental data [17] (opened square symbols) are also shown.

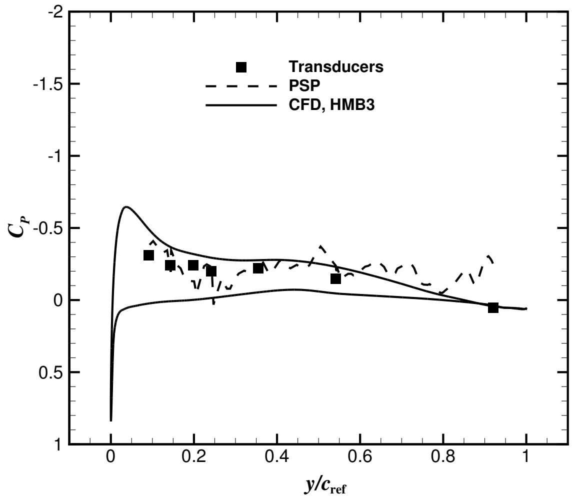

(a) C_T= 0.005.

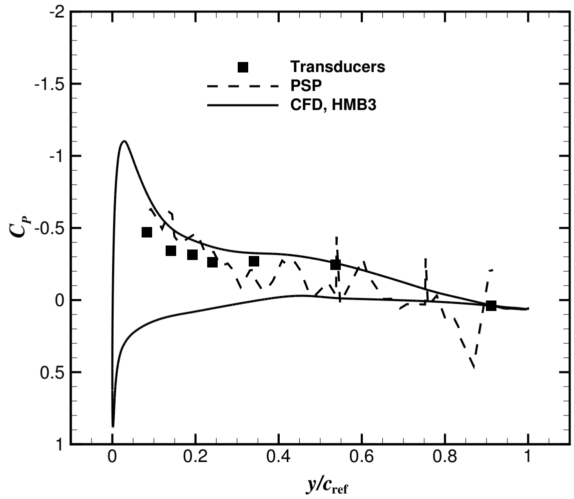

(b) C_T= 0.007.

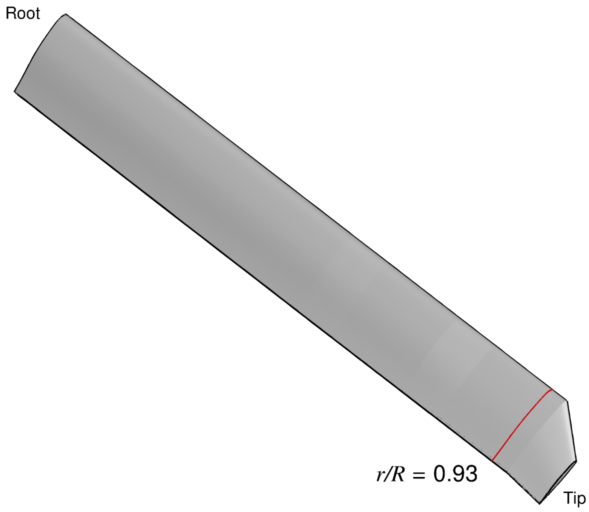

(c) Radial station.

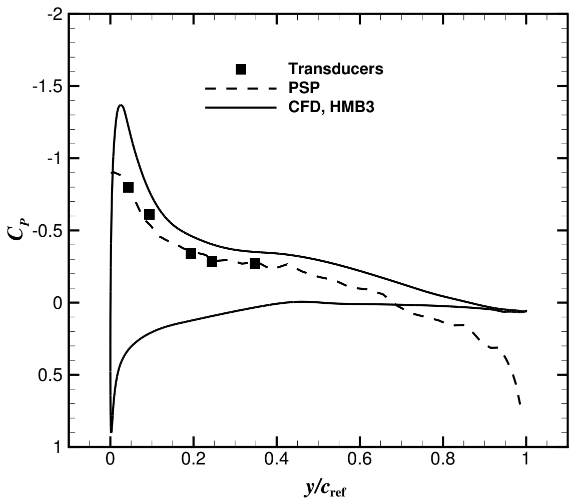

(d) C_T= 0.008.

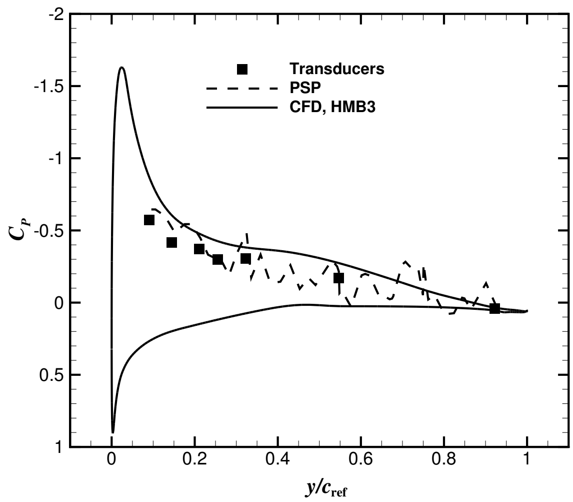

(e) C_T= 0.009.

Figure 5: C_P profile comparisons between experimental data using the PSP technique (dashed line) and pressure tap (square symbols) [15] and CFD (solid line) at radial station $r/R = 0.93$.

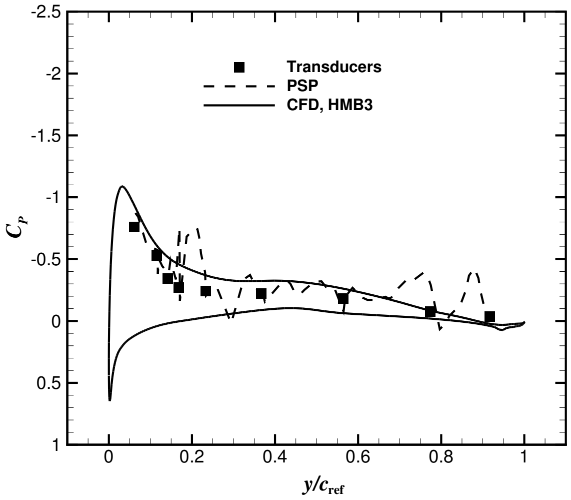

(a) C_T= 0.005.

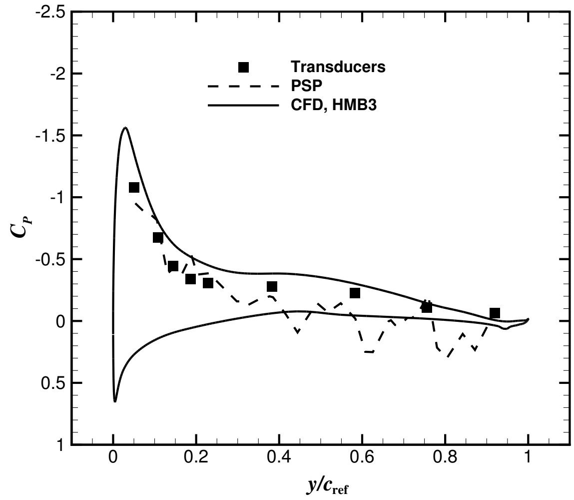

(b) C_T= 0.007.

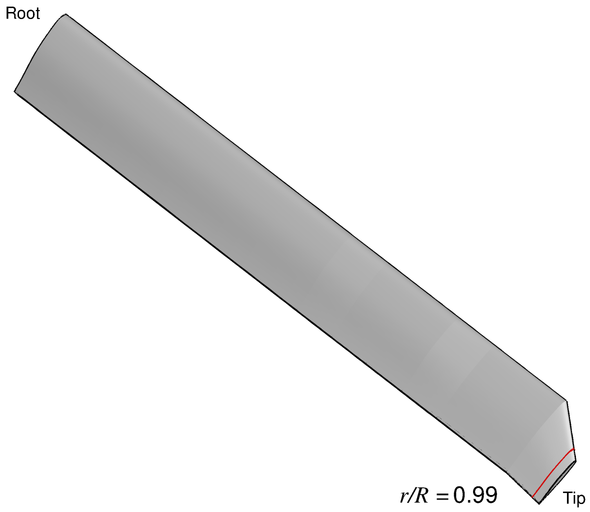

(c) Radial station.

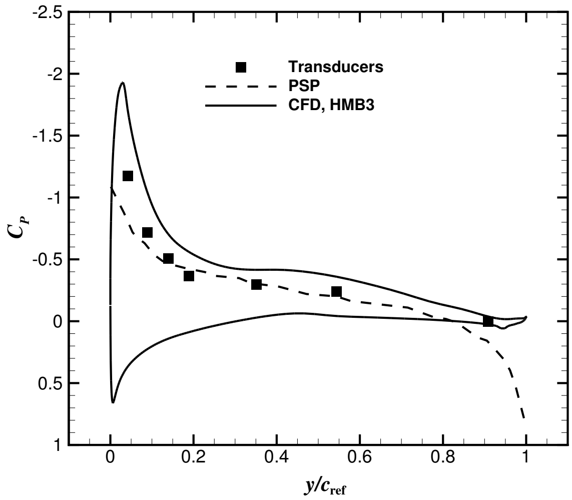

(d) C_T= 0.008.

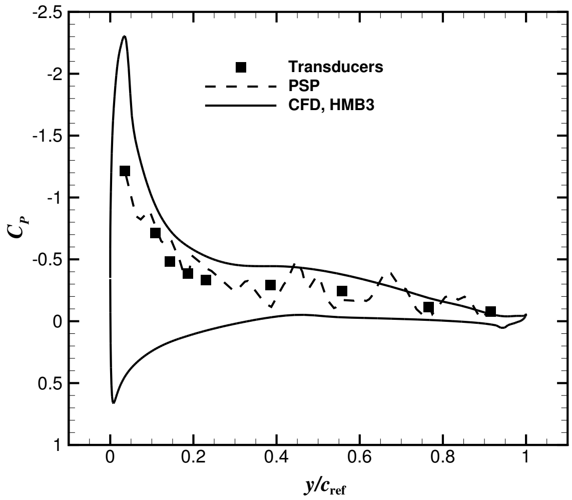

(e) C_T= 0.009.

Figure 6: C_P profile comparisons between experimental data using the PSP technique (dashed line) and pressure tap (square symbols) [15] and CFD (solid line) at radial station $r/R = 0.99$.

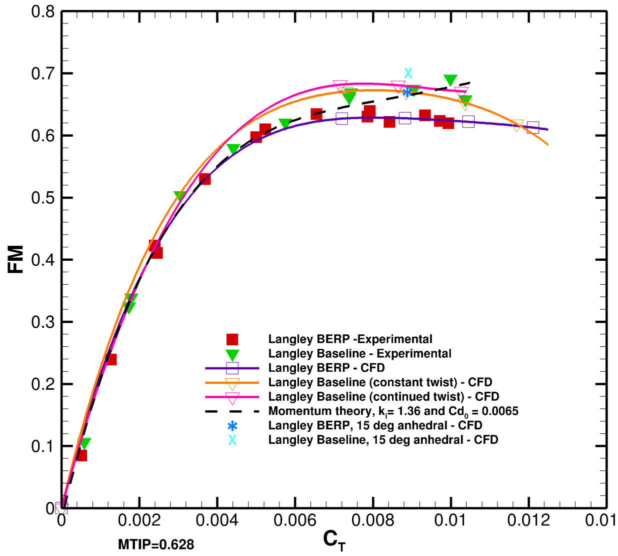

(a) C_T vs FoM

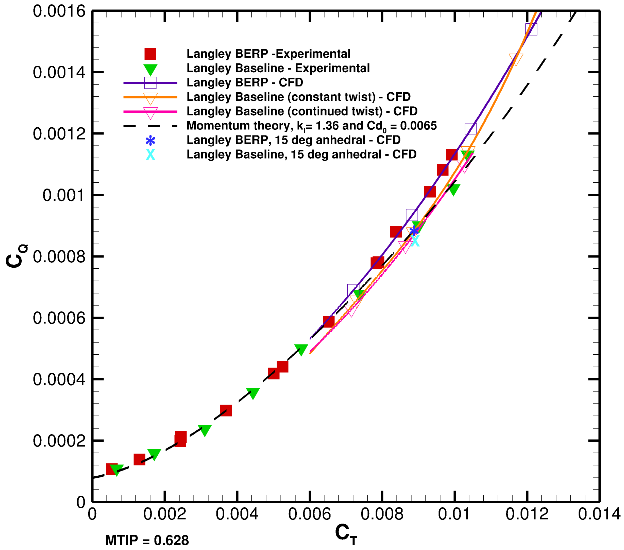

(b) C_T vs C_Q

Figure 7: Integrated loads predictions for the Langley BERP and Baseline blades and comparison with experimental data from Yeager et al. [22].

Table 4: Hover performance comparison of standard Langley BERP and Baseline blades, and blades with 15 degrees parabolic anhedral.

Blade	C_T	C_Q	FM	**FM % improvement**
LBASELINE	0.00885	0.000880	0.6702	-
LBERP	0.00882	0.000934	0.6276	-
LBASELINE with 15 deg anhedral	0.00891	0.000849	0.6997	+4.4%
LBERP with 15 deg anhedral	0.00888	0.000883	0.6698	+6.7%

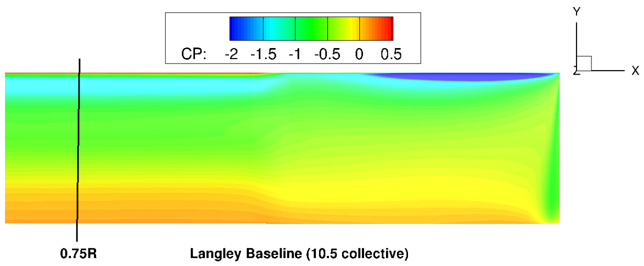

(a) LBASELINE blade

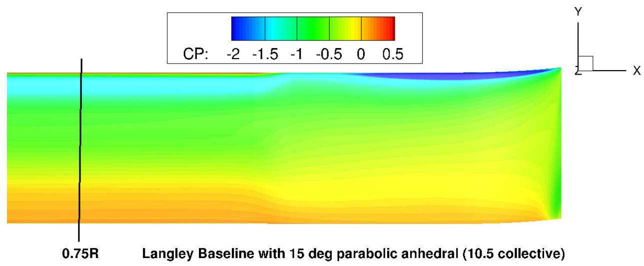

(b) LBASELINE blade with 15 deg anhedral

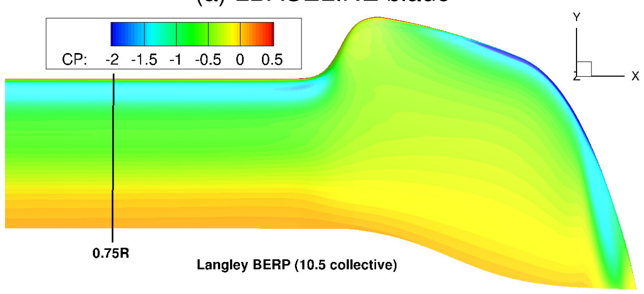

(c) LBERP blade

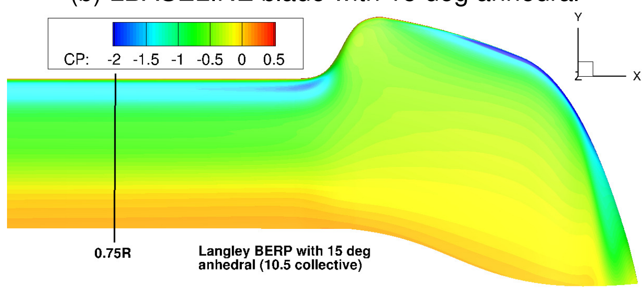

(d) LBERP blade with 15 deg anhedral

Figure 8: Comparison of surface pressure distributions (normalised by local flow velocity) for the Langley Baseline and BERP blades in hover with and without anhedral.

Table 5: Trim states for the PSP rotor in forward flight at three thrust levels.

C_T	Trimmed C_T	θ_s	θ_0	θ_{1s}	θ_{1c}	β_0	β_{1s}	β_{1c}
0.004	0.00406	6.0	6.117	4.536	-2.558	2.206	-0.501	-0.252
0.006	0.00600	6.0	8.324	6.840	-3.392	3.280	-0.643	-0.780
0.008	0.00804	6.0	10.560	8.956	-4.732	3.346	-1.171	-0.917

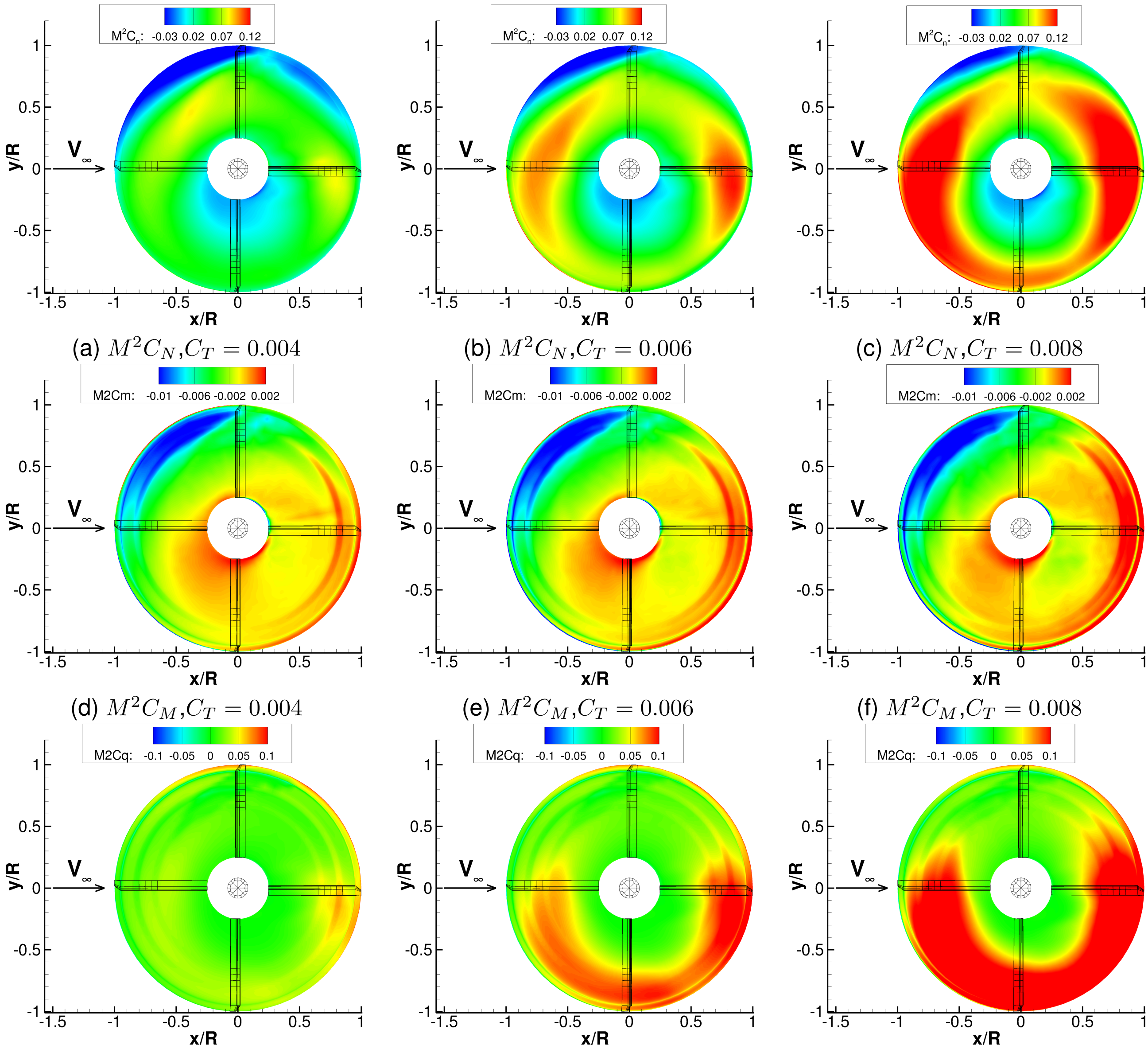

(a) M^2C_N,$C_T = 0.004$ (b) M^2C_N,$C_T = 0.006$ (c) M^2C_N,$C_T = 0.008$

(d) M^2C_M,$C_T = 0.004$ (e) M^2C_M,$C_T = 0.006$ (f) M^2C_M,$C_T = 0.008$

(g) M^2C_Q,$C_T = 0.004$ (h) M^2C_Q,$C_T = 0.006$ (i) M^2C_Q,$C_T = 0.008$

Figure 9: Predicted rotor disk loads for the PSP rotor in forward flight at advance ratio μ=0.35 at three thrust coefficients.

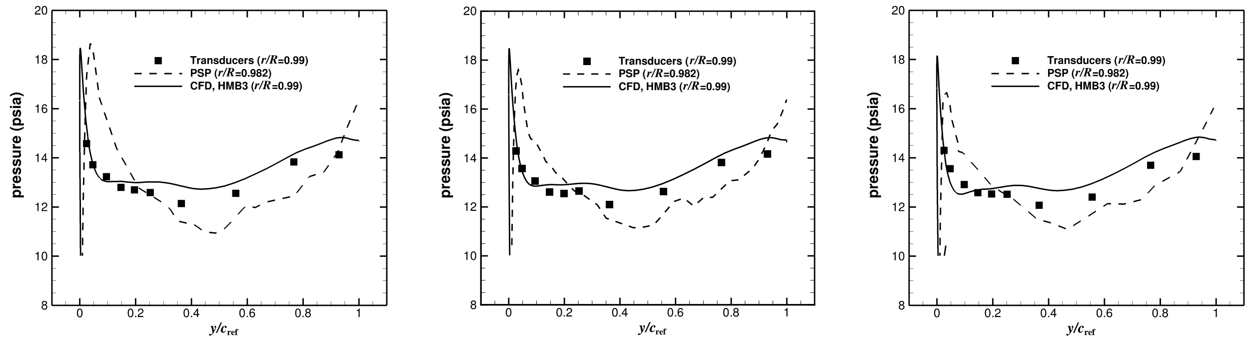

(a) ABS $\Psi = 101°$, $C_T = 0.004$ (b) ABS $\Psi = 101°$, $C_T = 0.006$ (c) ABS $\Psi = 101°$, $C_T = 0.008$

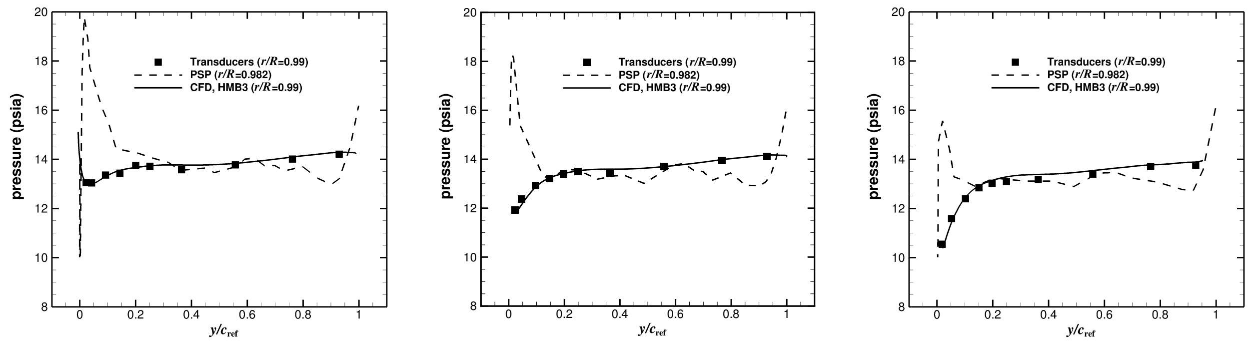

(d) RBS $\Psi = 262°$, $C_T = 0.004$ (e) RBS $\Psi = 262°$, $C_T = 0.006$ (f) RBS $\Psi = 262°$, $C_T = 0.008$

Figure 10: C_P profile comparisons between experimental data using the PSP technique (dashed line) and pressure tap (square symbols) [15] and CFD (solid line) at radial station $r/R = 0.99$. Pressure comparisons shown on advancing (ABS $\Psi = 101°$) and retreating blade side (RBS $\Psi = 262°$) at three thrust coefficients for PSP rotor in forward flight at advance ratio μ=0.35.

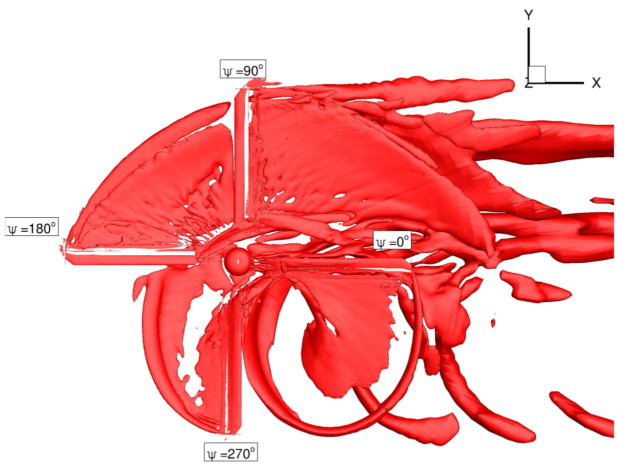

(a) $C_T = 0.004$

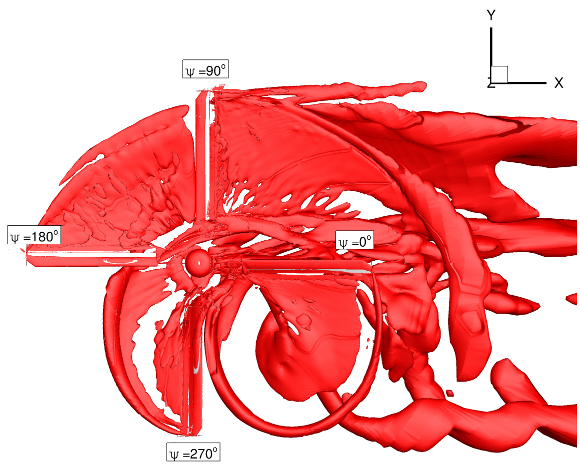

(b) $C_T = 0.008$

Figure 11: Wake visualisation for the low and high thrust cases using Q-criterion (value of 0.002) showing similar wake geometries for the PSP rotor in forward flight at μ=0.35.